Contribution of the turbulent heat fluxes to the summer melt of Saint-Sorlin glacier in the French Alps

Maxime Litt[1], Jean Emmanuel Sicart[1], Delphine Six[2] , Patrick Wagnon[1], and Warren Helgason[3]

[1] IRD/UJF-Grenoble 1/CNRS/G-INP, LTHE UMR 5564, Grenoble, France
[2] Laboratoire de Glaciologie et Géophysique de l'Environnement – Grenoble, UJF, France
[3] Civil and Geological Engineering, 57 Campus Drive, University of Saskatchewan, Saskatoon, Saskatchewan, Canada

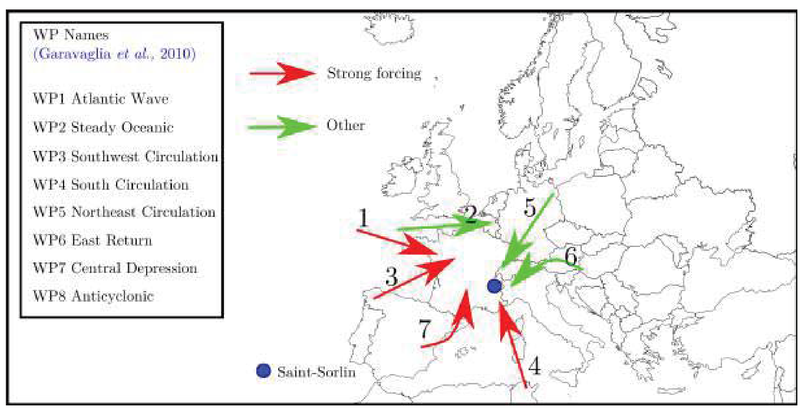

FIGURE 6.6 – Direction of the atmospheric flow in the lower atmospheric layers for different WP (adapted from Garavaglia *et al.*, 2010). (red arrows) Direction of the flow for the WP associated to strong forcing and (green arrows) direction of the flow for the other WP. No flow direction is shown for weak forcing conditions (WP8) since atmospheric wind speed was weak and direction ill-defined for these conditions.

TABLE 6.2 – Characteristics of the two field campaigns in terms of WP frequencies, meteorological data, turbulence and turbulence fluxes. Fraction of runs recorded under each group of WPs, fraction of GQR for the EC data in 2006, inside each group, and fraction of runs, inside each group during the 2009 campaign, for which a wind-speed maximum was observed with the profile mast. Mean meteorological variables recorded by the AWS-O, mean TKE in each weather group and turbulent fluxes measured with the EC and the BA methods with different roughness parameters.

	Strong Forcing		Weak forcing		Other	
	2006	2009	2006	2009	2006	2009
Time coverage	26%	46%	47%	32%	27%	21%
Fraction of GQR (EC)	85%	-	75%	-	12%	-
Fraction of GQR with a detected wind-speed maximum	-	31%	-	71%	-	72%
u_{AWS-O} [m s^{-1}]	5.2	5.5	2.5	2.6	3.0	2.6
T_{AWS-O} [°C]	7.2	9.1	7.6	5.3	2.9	4.4
q_{AWS-O} [kg kg^{-1}]	0.0049	0.0048	0.0058	0.0049	0.0048	0.0047
TKE [m^{-2} s^{-2}]	2.6	-	1.0	-	2.1	-
Fluxes [W m^{-2}]						
H_{EC}	45	-	24	-	21	-
LE_{EC}	-9	-	5	-	-9	-
$H_b(z_{0,t,q})$	33	41	16	7	12	5
$LE_b(z_{0,t,q})$	-6	-5	4	-3	-3	-2
$H_b(z_e)$	46	58	17	7	14	5
$LE_b(z_e)$	-9	-7	5	-4	-4	-3

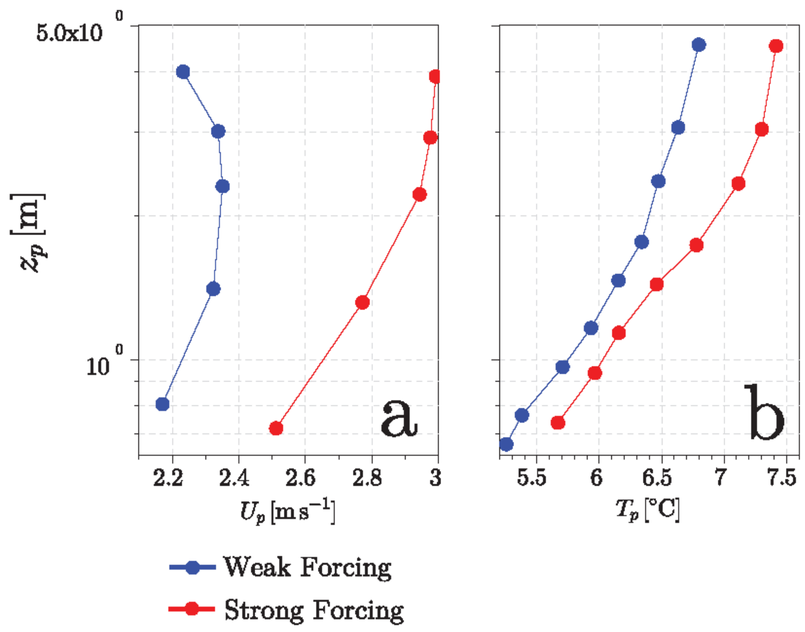

FIGURE 6.11 – (a) Median wind-speed profiles and (b) temperature profiles during the 2009 field campaign for (blue) Weak Forcing conditions and (red) Strong Forcing conditions.

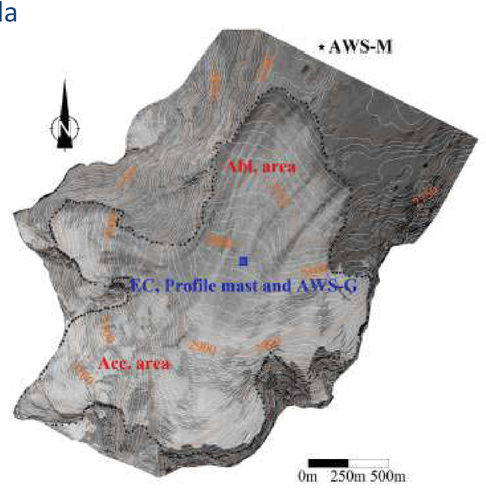

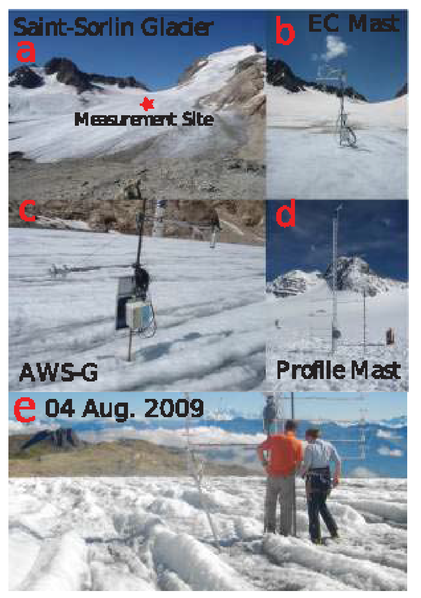

FIGURE 6.5 – Overview of the glacier and the instruments installed during the field campaigns. (left) Topographic map of the glacier and position of the instruments. (a) Picture of the Saint-Sorlin glacier taken from the AWS-M (heading to the top of the glacier, south is at the horizon), (b-c-d) the instruments installed during the 2006 and 2009 campaigns and (e) surface state at the end of the 2009 campaign.

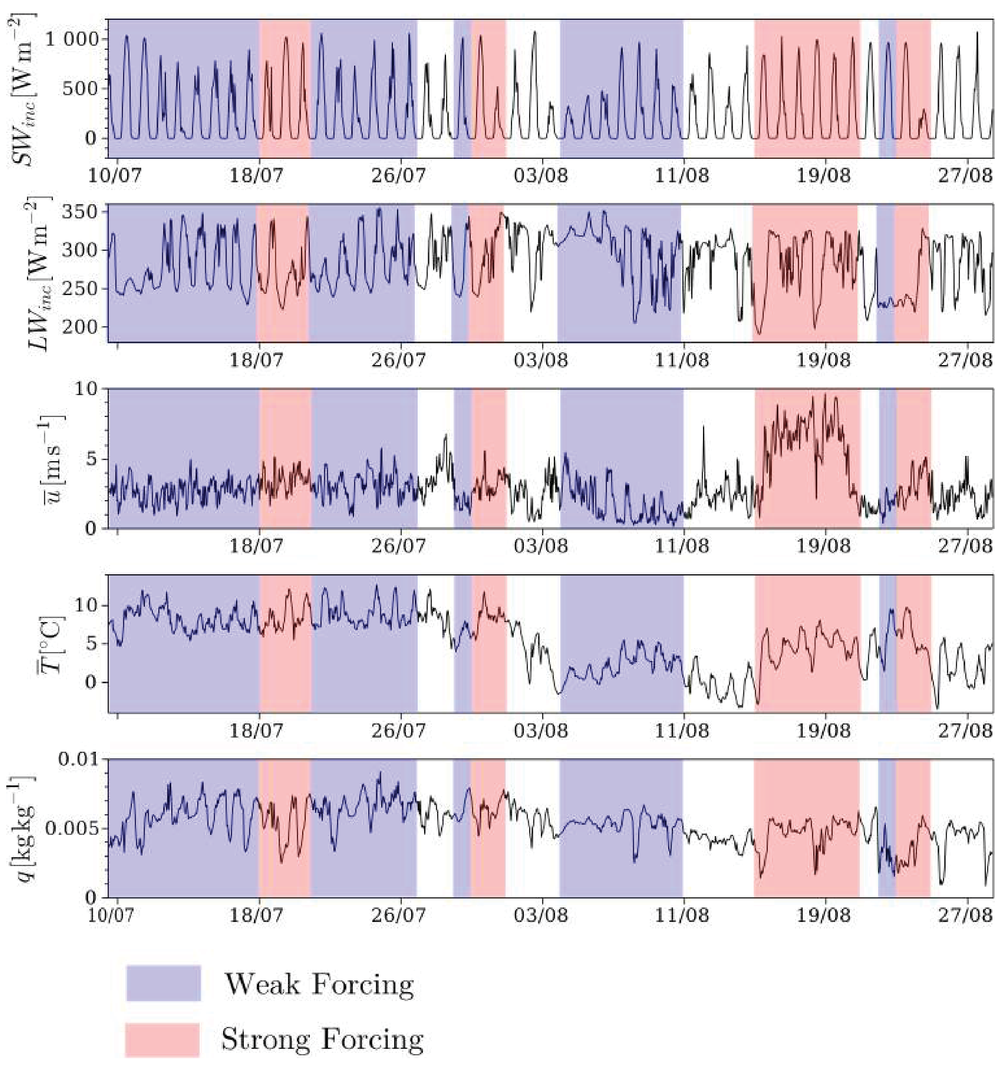

FIGURE 6.7 – Change of the meteorological variables in the ablation zone of the glacier at the AWS-G, during the 2006 field campaign. (a) incoming shortwave radiation, (b) incoming longwave radiation, (c) wind speed, (d) air temperature and (e) specific humidity of the air measured by the AWS-G. Strong Forcing conditions are shaded in red and Weak Forcing conditions in blue.

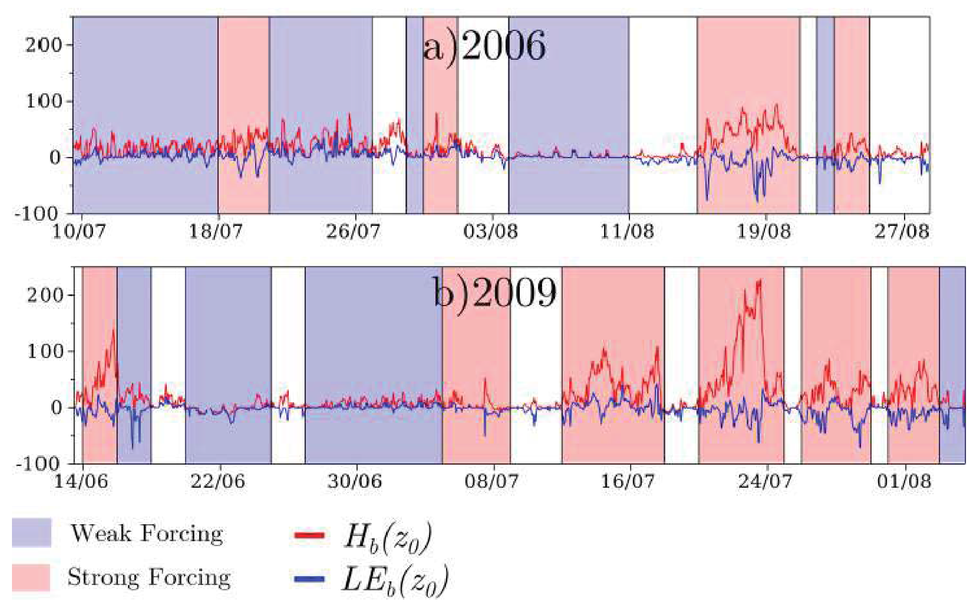

FIGURE 6.14 – Change of the turbulent flux evaluated with the BA method and the profile-derived roughness lengths, during (a) the 2006 field campaigns and (b) the 2009 field campaign. (red curve) The sensible heat fluxes and (blue curve) the latent heat fluxes are shown. The Weak Forcing conditions are shaded in blue and the Strong Forcing conditions are shaded in red.

During the summers 2006 and 2009, field measurement campaigns were undergone in the ablation zone of Saint-Sorlin Glacier, in the French Alps: Eddy-Covariance measurements in 2006 and temperature and wind-speed vertical profiles in 2009. We characterized the wind regimes and associated surface-layer turbulent flows in relation with large scale forcing, characterized from the weather pattern decomposition of Garavaglia *et al.* (2010). The turbulent fluxes were derived from the bulk aerodynamic (BA) and the Eddy-Covariance (EC) methods.

The sensible heat fluxes (*H>0*) were heating the surface, they were generally larger in magnitude than latent heat fluxes (*LE<0*) which represent, on average, a small loss of energy for the glacier.
When synoptic forcing was weak, a katabatic wind-speed maximum was frequently observed at low height (around 2 m, 74% of these conditions). The turbulent kinetic energy (TKE) was small (< 1 m^2 s^{-2}), and both *H* and *LE* remained small.
When synoptic forcing was strong, under the influence of low-pressure systems, the large-scale winds roughly aligned with the glacier flow. High wind speeds were observed on the glacier, the TKE was generally large (> 2 m^2 s^{-2}) and katabatic wind-speed maxima were not frequently observed below 5 m (<40% of the time). *H* was large (>100 W m^{-2}) due to high wind speeds. Sublimation (*LE* < 0) was not large because of humid air and *LE* did not canceled the energy gains in *H*, so that net *H* + *LE* was a significant energy input for the glacier.

In all conditions, **low frequency perturbations** were observed in the wind-speed high frequency signals. In weak synoptic forcing, they probably were related to oscillations of the katabatic flow, whereas in strong synoptic forcing, they seemed related to large-scale orographic disturbances. These low-frequency perturbations affected the turbulent momentum and heat fluxes in the surface layer.
These perturbations caused random errors on the EC and the BA fluxes when the synoptic forcing was weak. The averaged turbulent fluxes derived from both methods were quite similar and small.
The BA method systematically underestimated the fluxes when the synoptic forcing was strong and the TKE was large.

In warm and windy conditions, the melt rate of alpine glaciers may be underestimated when the turbulent fluxes are derived from profile aerodynamic methods.